

# Coupled-mode theory for the interaction between acoustic waves and spin waves in magnonic-phononic crystals: Propagating magnetoelastic waves

Piotr Graczyk\* and Maciej Krawczyk†

*Faculty of Physics, Adam Mickiewicz University in Poznan, Umultowska 85, 61-614 Poznan, Poland*

(Received 7 April 2017; revised manuscript received 8 June 2017; published 6 July 2017)

We have investigated codirectional and contradirectional couplings between spin wave and acoustic wave in a one-dimensional periodic structure (the so-called magphonic crystal). The system consists of two ferromagnetic layers alternating in space. We have taken into consideration materials commonly used in magnonics: yttrium iron garnet, CoFeB, permalloy, and cobalt. The coupled mode theory (CMT) formalism has been successfully implemented to describe the magnetoelastic interaction as a periodic perturbation in the magphonic crystal. The results of CMT calculations have been verified by more rigorous simulations with the frequency-domain plane-wave method and the time-domain finite-element method. The presented resonant coupling in the magphonic crystal is an active in-space mechanism which spatially transfers energy between propagating spin and acoustic modes, thus creating a propagating magnetoelastic wave. We have shown that CMT analysis of the magnetoelastic coupling is an useful tool to optimize and design a spin wave–acoustic wave transducer based on magphonic crystals. The effect of spin-wave damping has been included to the model to discuss the efficiency of such a device. Our model shows that it is possible to obtain forward conversion of the acoustic wave to the spin wave in case of codirectional coupling and backward conversion in case of contradirectional coupling. That energy transfer may be realized for broadband coupling and for generation of spin waves which are of different wavelength (in particular, shorter) than exciting acoustic waves.

DOI: [10.1103/PhysRevB.96.024407](https://doi.org/10.1103/PhysRevB.96.024407)

## I. INTRODUCTION

Coupled mode theory (CMT) is a well-known perturbation method in electromagnetism. It is used to describe coupling of modes in waveguides or Bragg reflections in periodic media [1]. In the limit of small perturbations CMT gives a simple picture of the underlying physical mechanisms, and thus it is complementary to more accurate numerical techniques like finite-element method. In particular, Solc filters, waveguide couplers, and distributed feedback resonators are analytically characterized by CMT [2–7].

When two modes are resonantly coupled, the energy is exchanged between them. We are interested in wave propagation phenomena, so in this paper we consider the coupling-in-space mechanism only. Then the modes may be coupled in two different ways, depending on their relative directions of the group velocities. In the case of contradirectional coupling, interacting modes have opposite signs of the group velocities and the phenomenon is similar to the Bragg reflection at the frequency from the stop band where the two dispersion branches of opposite slope anticross each other. Therefore, the mode that enters the area where the coupling mechanism exists becomes an evanescent wave passing the energy to the other mode. The outgoing reflected mode will be almost purely the other mode, providing that the distance of interaction is long enough. On the other hand, in codirectional coupling, the modes have the same signs of the group velocities and the complete conversion of energy from one mode to another occurs periodically in space in the forward direction at the distance defined by the coupling coefficient.

In this article we present the application of CMT formalism to the interaction of spin waves and acoustic waves in the so-called magphonic crystal. Magphonic crystal [8,9] is a periodic structure that is considered a phononic and magnonic crystal simultaneously, i.e., a system that is periodic both for acoustic waves and spin waves. Multiple crossings between spin-wave dispersion branches and acoustic-wave dispersion branches are present as a consequence of periodicity, i.e., a folding-back effect. This creates suitable conditions for co- and contradirectional couplings which do not exist in homogeneous materials.

The coupling mechanism between spin waves and acoustic waves is a magnetoelastic interaction (MEC), i.e., magnetostriction [10]. The dynamic magnetization which is related to the spin wave exerts dynamic strain in the material. On the other hand, the strain associated with the acoustic wave induces a dynamic effective magnetic field (inverse magnetostriction). If the strain field frequency (and its spatial distribution, i.e., wavelength) induced by the spin wave matches the frequency of the magnetic effective field induced by the acoustic wave, then the resonance criterion for the dynamic magnetoelastic coupling is satisfied.

The coupled equations of motion for spin wave and acoustic wave are given in Ref. [11]. It is possible to couple them in the linear regime only for acoustic waves that have a transverse component. This effect has been known for a homogeneous ferromagnetic material since the 1950s [12]. It is now intensively studied for standing waves [13], dynamic strain-mediated magnetization reversal [14], wave propagation [15–19], as well as in the femtosecond laser pump-laser probe experiments [20,21] or acoustic pump-laser probe experiments [22–25]. In Ref. [26] the transmission of acoustic energy through a nonmagnetic-ferromagnetic (Pt/yttrium iron garnet) interface at the vicinity of magnetoelastic anticrossing has been investigated theoretically. However, to have complete

\*graczyk@amu.edu.pl

†krawczyk@amu.edu.pl

picture of the mechanism, more rigorous dynamical description of magnetoelastic coupling in space is needed. Especially, if the goal is the effective transformation of propagating excitation from acoustic to magnetic or vice versa, then the spatial and temporal evolution of the excitations need to be investigated.

So far, only the crossing of acoustic wave band with almost dispersionless spin-wave band has been considered. This crossing acts as a band-gap for an acoustic wave but does not allow us to excite a propagating spin wave. Here, we show that it is possible to excite a propagating magnetoelastic wave by introducing codirectional coupling at higher magnetic fields. Then, we demonstrate that by optimization of the magphonic crystal structural parameters it is possible to achieve strong codirectional coupling also for a low magnetic field. Moreover, in the periodic system multiple contradirectional crossings are present which result in the formation of the stop bands both for spin wave and acoustic wave.

We have obtained the exact expression for the coupling coefficient in the magphonic crystal for anticrossings between spin-wave and acoustic-wave dispersion branches from different bands. We characterized the magnitude of the coupling as a function of the mode number and filling factor for magphonic crystals composed of different materials, i.e., yttrium iron garnet (YIG), CoFeB, cobalt, and permalloy, which are commonly used in magnonics. The results have been compared with the relevant dispersion relations obtained by the plane-wave method (PWM). The spatial evolution of magnetoelastic modes is shown for the co-directional and contradirectional couplings. The predictions of energy transfer length from acoustic wave to spin wave obtained by CMT are verified by the time-domain simulations (finite-element method). The effect of damping both in CMT and in time-domain simulations is taken into account and discussed for aforementioned phenomena. Finally, with the help of CMT and finite-element simulations, we optimize the magphonic crystal for bulk waves to act as a spin-acoustic wave transducer.

## II. COUPLED MODE THEORY FORMALISM

In the calculations the bulk spin wave with dynamic components of magnetization  $m_1$  and  $m_2$  (Fig. 1) is coupled linearly [11] to the transverse bulk acoustic wave described by the displacement  $u_3$ . Both waves propagate along the  $x_1$  direction. The magphonic crystal consists of alternating layers of isotropic ferromagnetic materials with the periodicity along  $x \equiv x_1$  described by lattice constant  $a$  and filling fraction  $f$ . The spin-wave dynamics is described by the Landau-Lifshitz equation for magnetization components  $m_1$  and  $m_2$ , which for propagation in the direction  $x$  and in the exchange regime takes the form:

$$\begin{aligned} \dot{m}_1 &= \omega_0 m_2 - \frac{\partial}{\partial x} \Lambda \frac{\partial m_2}{\partial x}, \\ \dot{m}_2 &= -\omega_0 m_1 + \frac{\partial}{\partial x} \Lambda \frac{\partial m_1}{\partial x}, \end{aligned} \quad (1)$$

while the acoustic wave dynamics is described by the wave equation for displacement  $u \equiv u_3$ :

$$\rho \ddot{u} = \frac{\partial}{\partial x} c \frac{\partial u}{\partial x}, \quad (2)$$

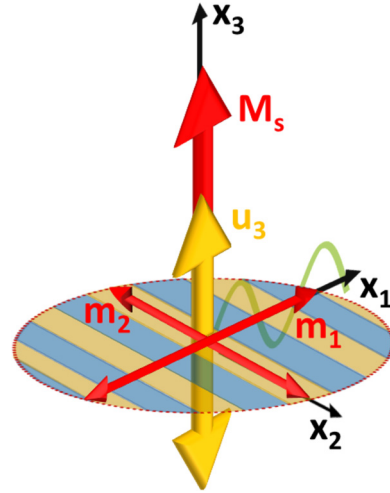


FIG. 1. The geometry of considered system. The transverse acoustic wave described by displacement  $u_3$  and the spin wave described by dynamic magnetization  $\vec{m} = (m_1, m_2)$  propagate along  $x_1$ , which is the direction of periodicity of the one-dimensional magphonic structure. The external magnetic field and thus saturation magnetization  $M_s$  is along  $x_3$ .

where  $\omega_0 = \gamma \mu_0 H$ ,  $\Lambda = 2A\gamma/M_s$ ,  $\gamma = 176$  GHz/T is the gyromagnetic ratio,  $A$  is exchange length,  $H$  is external magnetic field,  $M_s$  the saturation magnetization,  $\mu_0$  the magnetic susceptibility of vacuum,  $\rho$  the mass density, and  $c \equiv c_{44}$  is a component of the elastic tensor. The material parameters ( $A$ ,  $M_s$ ,  $c$ , and  $\rho$ ) taken into CMT calculations for the magphonic crystal are effective parameters except the magnetoelastic constant, which is periodic in space.

The solutions for homogeneous medium may be written in the form of normal modes  $\tilde{m}_{ij} \exp(k_j x - \omega t)$  and  $\tilde{u}_j \exp(q_j x - \omega t)$  indexed by wave vectors  $k_j$ ,  $q_j$  for spin modes and acoustic modes respectively at a given frequency  $\omega = 2\pi\nu$ ,  $i = 1, 2$ . The amplitudes  $\tilde{m}_{ij}$  and  $\tilde{u}_j$  are normalized here to unity. For the magphonic crystal:

$$\begin{aligned} k_j &= k_0 + G_{k_j}, \\ q_j &= q_0 + G_{q_j}, \end{aligned} \quad (3)$$

where  $k_0$  and  $q_0$  are wave vectors in the first Brillouin zone and  $G_{k_j}$ ,  $G_{q_j}$  are reciprocal lattice vectors. If  $k_0 = q_0$ , then it is a synchronous state; otherwise, it is an asynchronous state.

Now we couple Eqs. (1) and (2) by magnetoelastic terms proportional to  $B$ :

$$\begin{aligned} \dot{m}_1 &= \omega_0 m_2 - \Lambda \frac{\partial^2 m_2}{\partial x^2}, \\ \dot{m}_2 &= -\omega_0 m_1 + \Lambda \frac{\partial^2 m_1}{\partial x^2} - \gamma B \frac{\partial u}{\partial x}, \\ \rho \ddot{u} &= c \frac{\partial^2 u}{\partial x^2} + \frac{1}{M_s} \frac{\partial}{\partial x} B m_1. \end{aligned} \quad (4)$$

Then we express the solution of coupled equations as an expansion in the normal modes of the homogeneous medium:

$$\begin{aligned} m_i &= \sum_j M_j(x) \tilde{m}_{ij} e^{i(k_j x - \omega t)}, \\ u &= \sum_j U_j(x) \tilde{u}_j e^{i(q_j x - \omega t)}, \end{aligned} \quad (5)$$

where  $M_j(x)$  and  $U_j(x)$  are expansion coefficients which are dependent on  $x$ . Substituting to (4), taking into account Eqs. (1) and (2), and neglecting second derivatives on  $M_j$  and  $U_j$  leads to

$$2\Lambda \sum_j k_j \frac{\partial M_j}{\partial x} \tilde{m}_{1j} e^{ik_j x} = \gamma B \sum_j \left( q_j U_j - i \frac{\partial U_j}{\partial x} \right) \tilde{u}_j e^{iq_j x}, \quad (6a)$$

$$\begin{aligned} 2c \sum_j q_j \frac{\partial U_j}{\partial x} \tilde{u}_j e^{iq_j x} &= \frac{1}{M_s} \sum_j \left[ iB \frac{\partial M_j}{\partial x} \right. \\ &\quad \left. - \left( k_j B - i \frac{\partial B}{\partial x} \right) M_j \right] \tilde{m}_{1j} e^{ik_j x}. \end{aligned} \quad (6b)$$

Neglecting second derivatives is equivalent to the condition that  $M_j(x)$  and  $U_j(x)$  varies much slower in space than the wavelength of spin wave and acoustic wave (weak coupling approximation):

$$\begin{aligned} \frac{\partial^2 U_j}{\partial x^2} &\ll q \frac{\partial U_j}{\partial x}, \\ \frac{\partial^2 M_j}{\partial x^2} &\ll k \frac{\partial M_j}{\partial x}. \end{aligned} \quad (7)$$

Since the solutions of Eqs. (1) and (2) form set of orthogonal modes we can write relations:

$$\tilde{u}_j \cdot \tilde{u}_l^* = \delta_{jl}, \quad \tilde{m}_{1j} \cdot \tilde{m}_{1l}^* = \frac{1}{2} \delta_{jl}, \quad \tilde{m}_{1j} \cdot \tilde{u}_l^* = \frac{1}{\sqrt{2}}. \quad (8)$$

Using (8), we multiply Eq. (6a) by  $\tilde{m}_l^* e^{-ik_l x}$  and Eq. (6b) by  $\tilde{u}_l^* e^{-iq_l x}$  to get:

$$\begin{aligned} 4\Lambda k_l \frac{\partial M_j}{\partial x} &= \gamma B \sum_j \left( q_j U_j - i \frac{\partial U_j}{\partial x} \right) e^{i(q_j - k_l)x}, \\ 2cq_l \frac{\partial U_j}{\partial x} &= \frac{1}{M_s} \sum_j \left[ iB \frac{\partial M_j}{\partial x} - \left( k_j B - i \frac{\partial B}{\partial x} \right) M_j \right] e^{i(k_j - q_l)x}. \end{aligned} \quad (9)$$

The set of differential equations (9) describes coupled acoustic modes and spin modes. The strength of the coupling is expressed by magnetoelastic constant  $B$  which is periodic in space in magphonic crystal. Therefore, we can expand  $B$  into Fourier series with number  $n$  indexing reciprocal wave numbers  $G_n$ :

$$B = \sum_n b_n e^{-iG_n x} \quad (10)$$

and substitute into (9):

$$\begin{aligned} 4\Lambda k_l \frac{\partial M_j}{\partial x} &= \gamma \sum_n \sum_j b_n \left( q_j U_j - i \frac{\partial U_j}{\partial x} \right) e^{i(q_j - k_l - G_n)x}, \\ 2cq_l \frac{\partial U_j}{\partial x} &= \frac{1}{M_s} \sum_n \sum_j b_n \left[ i \frac{\partial M_j}{\partial x} - (k_j + G_n) M_j \right] \\ &\quad \times e^{i(k_j - q_l + G_n)x}. \end{aligned} \quad (11)$$

The effective coupling occurs only if the phase matching criterion is satisfied. If we consider interaction between  $k \equiv k_l$  and  $q \equiv q_j$  modes only, then the value of  $G \equiv G_n$  is fixed by the phase matching criterion to

$$G = q - k \text{ and } n = j - l, \quad (12)$$

which may be satisfied only in the synchronous state. Otherwise, in the asynchronous state, the phase difference  $\Delta q = q - k - G$  appears.

The magnetoelastic coupling is described now only by a single Fourier term  $b \equiv b_n$  [Eq. (10)] and the equations take the form (omitting subscript  $j$  at the  $M$  and  $U$ ):

$$\begin{aligned} \frac{\partial M}{\partial x} &= \left( a_1 U - ia_2 \frac{\partial U}{\partial x} \right) e^{i\Delta q x}, \\ \frac{\partial U}{\partial x} &= \left( ia_3 \frac{\partial M}{\partial x} - a_4 M \right) e^{-i\Delta q x}, \\ a_1 &= a_2 q, \quad a_2 = \frac{bM_s}{8Ak}, \\ a_3 &= \frac{b}{2cM_s q}, \quad a_4 = a_3(k + G). \end{aligned} \quad (13)$$

We substitute  $U \rightarrow U e^{-iqx}$ ,  $M \rightarrow M e^{-i(k+G)x}$  to get:

$$\begin{aligned} \frac{\partial M}{\partial x} &= \left[ i(k + G)M - ia_2 \frac{\partial U}{\partial x} \right], \\ \frac{\partial U}{\partial x} &= \left( iqU + ia_3 \frac{\partial M}{\partial x} \right). \end{aligned} \quad (14)$$

The general solution for a given values of  $M(0)$  and  $U(0)$  is

$$\begin{aligned} M(x) &= e^{-i\bar{\beta}x} \left\{ \left[ \cos(Dx) + i \frac{\Delta\beta}{D} \sin(Dx) \right] M(0) \right. \\ &\quad \left. + \frac{\kappa_{12}}{D} \sin(Dx) U(0) \right\}, \\ U(x) &= e^{-i\bar{\beta}x} \left\{ \left[ \cos(Dx) - i \frac{\Delta\beta}{D} \sin(Dx) \right] U(0) \right. \\ &\quad \left. - \frac{\kappa_{21}}{D} \sin(Dx) M(0) \right\}, \end{aligned} \quad (15)$$

where

$$\begin{aligned} \bar{\beta} &= \frac{G + k + q}{2}, \quad \Delta\beta = \frac{G + k - q}{2}, \\ |\kappa_{12}| &= \frac{bM_s q}{8Ak}, \quad |\kappa_{21}| = \frac{b(k + G)}{2cqM_s}, \\ \kappa &= \sqrt{\kappa_{12}\kappa_{21}} = \mp \frac{b}{4} \sqrt{\frac{k + G}{Ack}}, \\ D &= \sqrt{\Delta\beta^2 - \kappa^2}, \end{aligned} \quad (16)$$

where the upper sign for  $\kappa$  codirectional coupling and lower sign is for contradirectional coupling, which comes from the fact that  $\kappa_{12}$  and  $\kappa_{21}$  are imaginary or real, respectively [3]. Since the coupling coefficient  $\kappa$  describes how fast the amplitudes  $M(x)$  and  $U(x)$  vary in space, the results of CMT calculations are valid under conditions [weak-coupling approximation, Eq. (7)]

$$\kappa \ll k \text{ and } \kappa \ll q. \quad (17)$$

The wave vectors of coupled modes in the region close to the resonance are

$$\begin{aligned} \beta_1 &= \bar{\beta} + D, \\ \beta_2 &= \bar{\beta} - D. \end{aligned} \quad (18)$$

Dispersion relations of the coupled modes can be obtained close to the crossings by calculating new wave numbers  $\beta_1$  and  $\beta_2$  from Eqs. (18) for a given frequency  $\omega$ . The values of  $k$  and  $q$  are taken for the same frequency from the dispersion relations of the uncoupled spin wave and acoustic wave, respectively.

### A. Codirectional coupling

The solutions of Eqs. (15) for the boundary conditions  $M(0) = 0$  and  $U(0) = U_0$ , i.e., when the wave is at the starting point purely acoustic mode, are

$$\begin{aligned} M(x) &= U_0 \frac{\kappa_{12}}{D} \sin(Dx) e^{-i\bar{\beta}x}, \\ U(x) &= U_0 \left[ \cos(Dx) - i \frac{\Delta\beta}{D} \sin(Dx) \right] e^{-i\bar{\beta}x}. \end{aligned} \quad (19)$$

The magnetic and acoustic modes are both sine or cosine modulated traveling waves  $\exp(-i\bar{\beta}x)$ .

$$\begin{aligned} M(x) &= U_0 \frac{\kappa_{21}}{T} \frac{\cosh TL \sinh T(x-L) - i \frac{\Delta\beta}{T} \sinh TL \sinh T(x-L)}{1 + \frac{\kappa_{12}^2}{T^2} \sinh TL} e^{-i\bar{\beta}x}, \\ U(x) &= U_0 \frac{\cosh Tx - \frac{\kappa_{12}^2}{T^2} \sinh TL \sinh T(x-L) - i \frac{\Delta\beta}{T} \sinh Tx}{1 + \frac{\kappa_{12}^2}{T^2} \sinh TL} e^{-i\bar{\beta}x}. \end{aligned} \quad (23)$$

The spin and acoustic modes are both traveling waves  $\exp(-i\bar{\beta}x)$  modulated by hyperbolic sine or hyperbolic cosine. Contradirectional coupling is possible for the periodic structure, when the folding-back effect occurs and the signs of  $q$  and  $k$  are opposite. Then the coupling is described by higher Fourier coefficients of  $B$  in the form:

$$b = b_n = \frac{B_1 - B_2}{\pi n} \sin(n\pi f). \quad (24)$$

## III. RESULTS

First, in Sec. III A we give the description of the spin wave–acoustic wave coupling in the homogeneous ferromagnetic medium. Then the periodicity of the magnetoelastic constant in the magphonic crystal that consists of alternating permalloy  $\text{Ni}_{77}\text{Fe}_{23}/\text{Ni}_{85}\text{Fe}_{15}$  (Py1/Py2) layers is introduced in Sec. III B and CMT results are discussed. It is assumed

We will consider codirectional couplings for the first bands of spin wave and acoustic wave in the homogeneous material ( $j = l = n = 0$ ) and in the magphonic crystal. Then  $k = k_0$ ,  $q = q_0$ , and  $G = 0$ . Magnetoelastic interaction is described here by the zeroth Fourier coefficient, i.e., the magnetoelastic constant has a value as for an effective homogeneous medium:

$$b = b_0 = B_1 f + B_2(1 - f), \quad (20)$$

where  $f$  is the structure filling fraction with the material 1. In the synchronous state the coupling coefficient has a maximum magnitude which is

$$\kappa_{\max} = \frac{b}{4\sqrt{Ac}}. \quad (21)$$

The energy transfer length  $L_{\text{tr}}$  from the acoustic mode to the spin mode is defined from zeroing the cosine in Eq. (19) which gives for a synchronous state:

$$\kappa L_{\text{tr}} = \frac{\pi}{2}. \quad (22)$$

It is worth noting that since  $D$  has higher values for the asynchronous state [ $\Delta\beta \neq 0$  in Eq. (16)], the transfer of energy is more frequent in space than in the synchronous state, but the total power exchanged between the modes decreases.

### B. Contradirectional coupling

In contradirectional coupling the value of  $D$  in Eq. (16) becomes imaginary for the synchronous state. The solution of Eqs. (15) with the substitution  $T = iD$  and the boundary conditions  $M(L) = 0$  and  $U(0) = U_0$ , i.e., when the spin mode is supposed to have zero amplitude at the distance  $L$  is

that all other material parameters are the same between the layers. Next, we consider permalloy-cobalt magphonic crystal. In our model the magnetoelastic constant varies periodically in space while other material parameters are taken as for effective homogeneous medium. We compare the results of the CMT with the plane-wave method in frequency domain and with finite-element time-domain simulations. Details of PWM calculations are given in Ref. [27]. Finally, in Sec. III C, we discuss the effect of spin-wave damping onto the multilayer optimized for acoustic wave–spin wave conversion.

### A. Codirectional coupling in homogeneous material

To present the codirectional mode coupling in a homogeneous medium we chose CoFeB in the high magnetic field of 1 MA/m, for which the weak coupling condition (17) is satisfied. Figure 2(a) presents a dispersion relation at the vicinity of the anticrossing obtained from CMT calculations

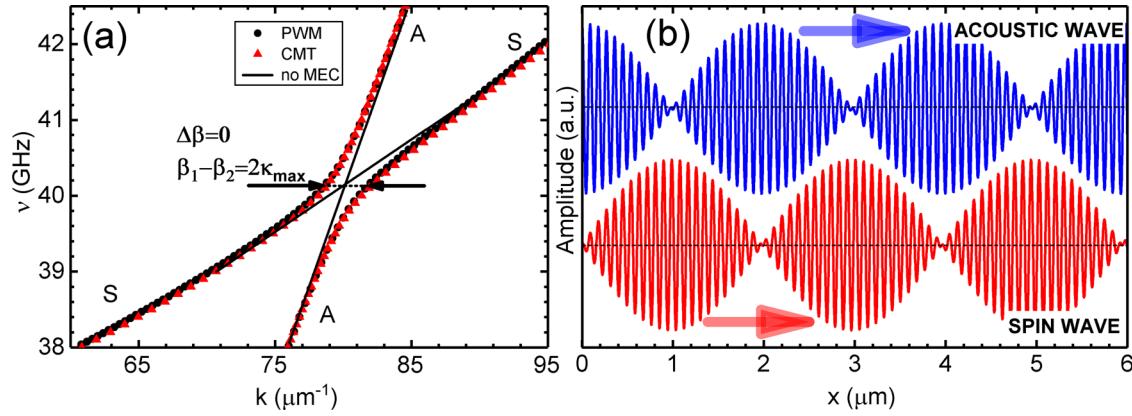


FIG. 2. (a) Codirectional anticrossing of acoustic wave (A) and spin wave (S) in CoFeB calculated by CMT (red triangles) and PWM (black dots). Solid lines mark dispersion relations in the absence of magnetoelastic coupling. Arrows mark the definition of coupling coefficient  $\kappa_{\max}$ . (b) Spatial distribution of acoustic-wave displacement  $u$  and spin-wave dynamic magnetization  $m_1$  in the codirectional coupling in CoFeB. Arrows indicate the propagation direction of waves.

and compared with the PWM method. Both results are in good agreement. Figure 2(b) shows the space variation of the spin-wave dynamic magnetization component  $m_1$  and acoustic-wave displacement  $u$  [Eq. (4)] in the point of the maximum coupling (synchronous state). The acoustic wave is transformed into a spin wave at a distance of about  $1 \mu\text{m}$ . Then, the spin wave is transformed back to the acoustic wave. This repetitive forward transformations create a propagating magnetoelastic wave. We have obtained the same space evolution by finite-element method time-domain simulations (see Sec. III C), contrary to the case of low magnetic fields in Ref. [26] (and long wavelengths), where, although the energy transfer occurs, the spin excitation does not propagate because of zero group velocity (flat dispersion relation) and the crossing acts effectively as a band gap for the acoustic wave.

In Table I we correlated the parameters of four most popular materials exploited in magnonics: yttrium iron garnet (YIG), CoFeB, Py, and Co. The maximum value of the coupling coefficient calculated from (22) is for Co and CoFeB, which give the transfer length  $L_{\text{tr}}$  for materials of about  $0.8 \mu\text{m}$  and  $1 \mu\text{m}$ , respectively. The transfer length is compared with the loss length  $L_{\text{loss}}$ , which is the distance at which the amplitude of the wave decays by the factor of  $1/e$  of the initial value. In the

TABLE I. Physical parameters of ferromagnetic materials and comparison of their magnetoelastic properties with the damping properties. Values of  $L_{\text{loss}}$  are given for  $\nu = 60 \text{ GHz}$ .

	YIG	CoFeB	Py	Co
$M_s$ (kA/m)	140 [28]	1150 [29]	860 [30]	1000 [31]
$A$ (pJ/m)	4 [28]	15 [29]	13 [30]	20 [32]
$c$ (GPa)	76	70	50	80
$\rho$ (kg/m <sup>3</sup> )	5110	7050	8720	8900
$B$ (MJ/m <sup>3</sup> )	0.55 [33]	6.5 [34]	$\pm 0.9^a$ [35]	10 [31]
$\kappa$ (1/ $\mu\text{m}$ )	0.36	2.36	0.4	3.03
$L_{\text{tr}}$ ( $\mu\text{m}$ )	6.22	1.0	5.62	0.8
$\alpha$	0.0003 [36]	0.004 [29]	0.01 [37]	0.1 [37]
$L_{\text{loss}}$ ( $\mu\text{m}$ )	40	1.8	0.8	0.09

<sup>a</sup>Minus sign for Py1, plus sign for Py2.

consideration of the effect of damping, we assumed that the acoustic wave is attenuated much smaller than the spin wave and this attenuation may be neglected. It is usually correct if we compare magnetic damping coefficients with acoustic ones for shear waves in metals [38,39]. For bulk spin wave  $L_{\text{loss}}$  is estimated from damping coefficient  $\alpha$  by the formula [28]:

$$L_{\text{loss}} = v_g \tau = \frac{4A\gamma k}{M_s \omega \alpha}, \quad (25)$$

where  $v_g$  is group velocity and  $\tau$  is relaxation time. Thus, for the coupling-in-space mechanism, a high lifetime of a spin wave together with high group velocity is crucial. The comparison gives the conclusion that the effect of the energy transfer is completely suppressed by the spin damping in the case of Co and Py. Only for CoFeB and YIG does the wave have a chance to transfer from spinlike to acoustic-like before being attenuated. Moreover, using high magnetic fields (in order to achieve high propagation velocities at the point of crossing as shown above for CoFeB) is somehow problematic from the point of view of applications. But the latter problem may be overcome in a periodic system.

## B. Contradirectional coupling in periodic structure

By introducing periodicity in the medium it is possible to achieve contradirectional couplings of the spin modes with the acoustic modes [27]. We considered the propagation perpendicular to the interfaces of alternating layers (layer thickness  $25 \text{ nm}$ ,  $a = 50 \text{ nm}$ ,  $f = 0.5$ ) of  $\text{Ni}_{77}\text{Fe}_{23}$  (Py1) and  $\text{Ni}_{85}\text{Fe}_{15}$  (Py2) alloys. The physical parameters of Py1 are given in Table I. We assumed that Py2 differs from Py1 only by the sign of the magnetoelastic constant. This can be done by choosing nickel-iron alloys of different composition [35]. Then the periodicity of the sample is solely due to periodicity of the magnetostriction.

Figure 3(a) shows the crossing C2 (see Table II) of the first acoustic mode ( $j = 0$ ) with the second spin mode ( $l = -1$ ) of the Py1/Py2 magnonic crystal for the external magnetic field  $H = 100 \text{ kA/m}$ . Clearly, at the frequency of about  $12 \text{ GHz}$  the band gap appears. The results of CMT analytical calculations are in good agreement with PWM simulations.

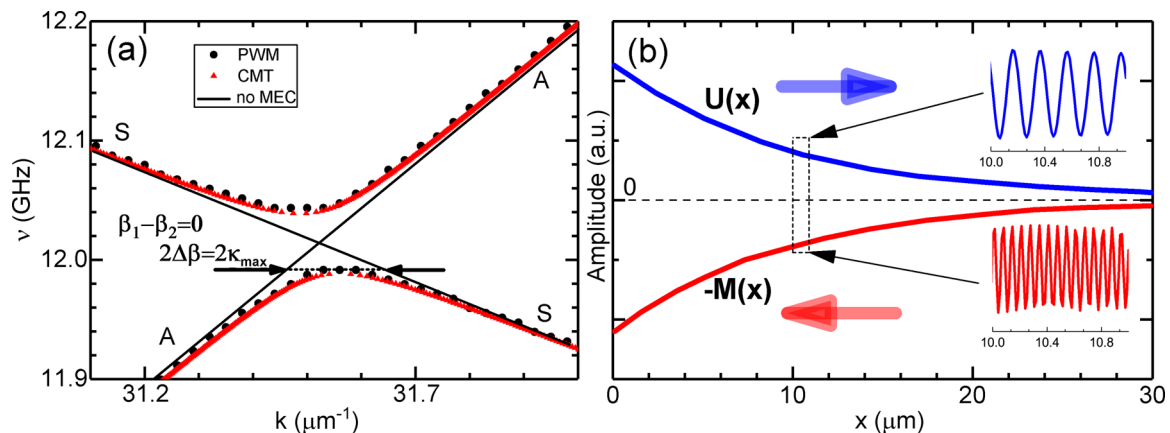


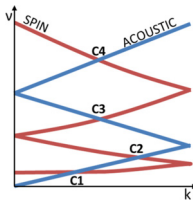
FIG. 3. (a) Contradirectional C2 anticrossing of acoustic wave (A) and spin wave (S) in Py1/Py2 calculated by CMT (red triangles) and PWM (black dots). Solid lines mark dispersion relations in the absence of magnetoelastic coupling. Arrows mark the definition of coupling coefficient  $\kappa_{\max}$ . (b) Spatial distribution of amplitudes  $U(x)$  and  $M(x)$  in the contradirectional coupling in Py1/Py2. Arrows indicate the propagation direction of waves. Insets show acoustic-wave displacement  $u$  and spin-wave dynamic magnetization  $m_1$  in the fragment of the structure.

The amplitudes of  $M(x)$  and  $U(x)$  obtained from Eq. (23) show [Fig. 3(b)] that the wave undergoes Bragg reflection together with the transformation from the acoustic-like to the spinlike. The amplitude of the acoustic wave propagating into the periodic system decays exponentially, while the amplitude of the backward-propagating spin wave increases. However, the distance which is needed to achieve sufficiently strong energy transfer is in the order of tens of micrometers. What is also worth noting is that the generated spin mode wavelength is shorter than the exciting acoustic mode, which is the result of crossing of dispersion branches of different number.

The magnitude of coupling coefficient  $\kappa$  has been calculated from Eq. (16) in dependence on the filling factor for the four consecutive crossings labeled C1, C2, C3, and C4 (see Table II) of the Py1/Py2 structure. The lattice constant of the structure is fixed to 50 nm and the filling factor indicates the percentage of Py2 in the system. The coupling coefficient has been determined also from the PWM dispersion relations in the way shown in Fig. 2(a) and Fig. 3(a) [compare with Eq. (18)]. The results are shown in Fig. 4. The coupling coefficient for the succeeding crossings obeys the relation of the succeeding Fourier terms  $b_n$  [Eq. (20) and Eq. (24)] what is not surprising since  $\kappa$  is proportional to the magnetoelastic constant. However, the CMT calculations fully agree with more rigorous numerical calculations, despite the fact that only the interaction of two modes are taken into account.

TABLE II. The mode numbers of acoustic wave ( $j$ ) and spin wave ( $l$ ) and respective number  $n$  for particular crossing.

	$j$	$l$	$n = j - l$
C1	0	0	0
C2	0	-1	1
C3	-1	1	-2
C4	1	-2	3



Next, we consider the C2 crossing of Py1/Co periodic structure of same structural parameters as previously (layer thickness 25 nm,  $a = 50$  nm,  $f = 0.5$ , and magnetic field  $H = 100$  kA/m). The magnetoelastic coefficient vary periodically in space, while all other physical parameters ( $A$ ,  $c$ ,  $M_s$ ,  $\rho$ ) of material are calculated as for effective homogeneous medium. The comparison of C2 crossing from CMT and PWM is shown in Fig. 5(a). Clearly, the anticrossing calculated by CMT is shifted in wave number and frequency due to the shift of acoustic branch of effective medium with respect to the right position of the acoustic branch obtained by PWM. Thus it seems that while the effective medium approximation works well for the spin wave, it is not the case for acoustic waves.

In Fig. 5(b) the Bragg reflection together with conversion from acoustic mode to spin mode and wavelength change is presented by CMT for this anticrossing. Much smaller multilayer thickness is needed for this conversion compared to

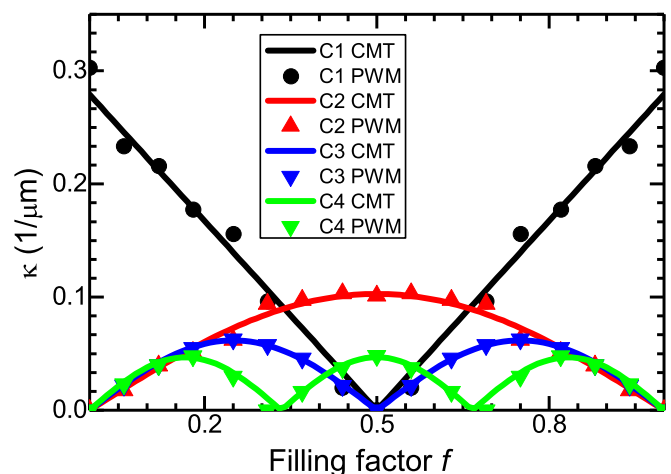


FIG. 4. Dependence of coupling coefficient  $\kappa$  on the filling factor  $f$  in the Py1/Py2 magphonic crystal for the four different crossings. The lines are result of CMT calculations, while the points come from PWM simulations.

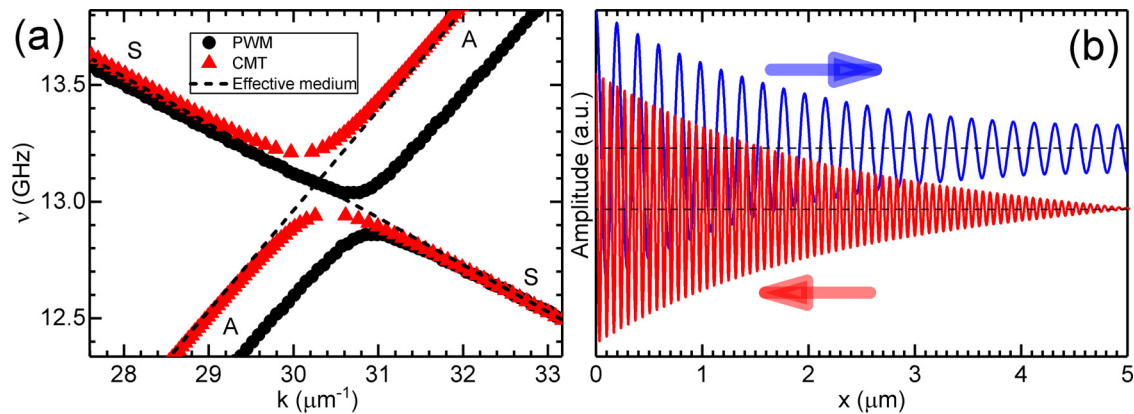


FIG. 5. (a) Contradirectional C2 anticrossing of acoustic wave (A) and spin wave (S) in Py1/Co calculated by CMT (red triangles) and PWM (black dots). Dashed lines mark dispersion relations for the effective medium in the absence of magnetoelastic coupling. (b) Spatial distribution of acoustic-wave displacement  $u$  and spin-wave dynamic magnetization  $m_1$  in the contradirectional coupling in Py1/Co. Arrows indicate the propagation direction of waves.

previous structure [Fig. 3(b)] as a consequence of much bigger magnetostriction in Co.

The coupling coefficient  $\kappa$  for Py1/Co changes with filling factor in a similar way as for the Py1/Py2 system and is determined by  $b_n$  (Fig. 6). However, the maxima in the C2, C3, and C4 crossings are no more symmetrical and they have a smaller maximum for a higher filling factor (more cobalt). For example, the maximum of  $\kappa$  for the C2 crossing is for the  $f = 0.45$ , which is the consequence of changing the effective material parameters [ $A$  and  $c$  in Eq. (21)] of the medium with the filling factor.

The comparison of CMT with PWM reveals that although the qualitative dependence of the coupling coefficient is reproduced by CMT, it quantitatively gives overestimated values of  $\kappa$ , especially for high values of the filling factor. For high filling with cobalt, it seems that effective medium approximation is not accurate. However, by taking other modes into account or expanding parameters into Fourier series, one can easily fit to PWM, but one also loses the most

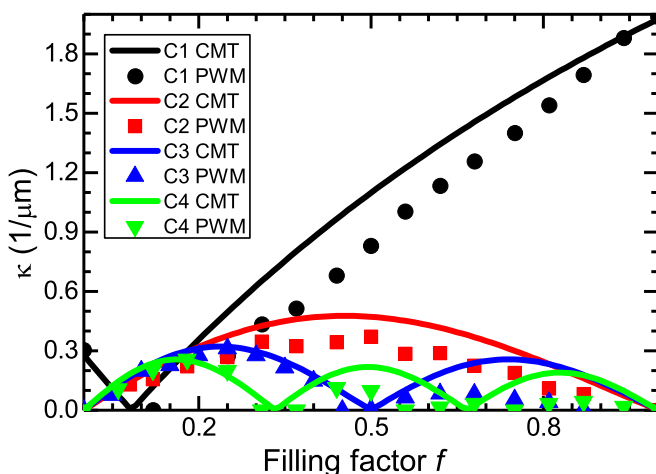


FIG. 6. Dependence of coupling coefficient  $\kappa$  on the filling factor  $f$  in the Py1/Co magphonic crystal for the four different crossings. The lines are result of CMT calculations, while the points come from PWM simulations.

important advantage of CMT, which is its simplicity and physical transparency.

### C. Time-domain simulations and the effect of damping

Since we deal with the coupling-in-space mechanism, it is important to consider the acoustic wave–spin wave transfer length together with the effect of damping. As mentioned in Sec. III A, the damping of spin waves in cobalt is very high and for  $\alpha = 0.1$  gives the loss length  $L_{\text{loss}} = 90$  nm for a bulk wave with a frequency of 60 GHz. This is a distance that is much smaller than the transfer length (Table I), so the energy transfer due to the magnetoelastic effect is completely suppressed. On the other hand, CoFeB has much lower damping together with a comparable value of the magnetoelastic constant. Therefore, we solved Eqs. (4) in time-domain finite-element simulations for Py1/CoFeB instead of a Py1/Co multilayer structure.

The Py1/CoFeB multilayer parameters were optimized to get broad codirectional coupling of spin and acoustic branches [Fig. 7(a)]. This was achieved for a lattice constant of 55 nm and an external magnetic field of 160 kA/m. For those values, the third acoustic branch ( $j = 1$ ) overlaps with the fifth spin branch ( $l = 2$ ) of the dispersion relation (see Table II) and we obtain broadband magnetoelastic coupling. The details of this optimization and plane-wave method calculations with magnetoelastic coupling are described in Ref. [27]. The strength of the coupling for the branches is also quite strong since the difference between the spin wave number and the acoustic wave number is of the one reciprocal lattice vector [ $n = -1$  in Eq. (12)]. Thus, the coupling coefficient changes with the filling factor similarly as for C2 crossing (compare Table II) in Fig. 4 and it becomes maximum for  $f = 0.47$ .

The transfer length for the Py1/CoFeB structure is calculated by CMT from Eqs. (16), (22), and (24) to be  $L_{\text{tr}} = 3.3$   $\mu\text{m}$ . We constructed in COMSOL Multiphysics the multilayer of thickness more than twice that distance, i.e., 7  $\mu\text{m}$ . The acoustic wave of 60 GHz is continuously excited at the point indicated by S [Fig. 7(b)]. Both spin and acoustic wave are damped at the edges of the simulated area to avoid reflections. The results of time-domain simulations described by Eqs. (4) are shown in Fig. 7(b) after 10 ns of excitation.

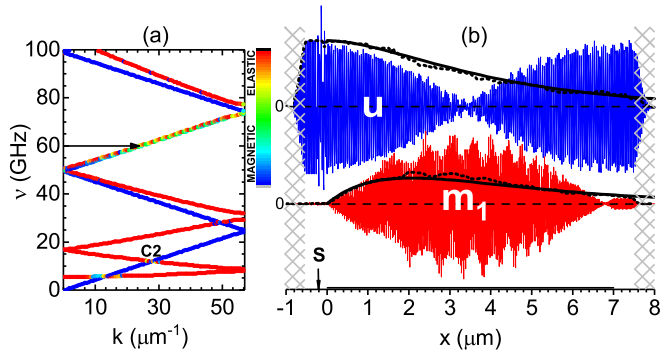


FIG. 7. (a) Dispersion relation for Py1/CoFeB magphonic crystal optimized for codirectional coupling obtained by PWM simulations. (b) Spatial distribution of acoustic displacement  $u$  (top) and spin-wave dynamic magnetization  $m_1$  (bottom) in the codirectional coupling in Py1/CoFeB. Blue and red are oscillations without damping; black dashed lines and solid lines are absolute amplitudes of the waves with damping from FEM simulations and CMT calculations, respectively. Black horizontal line at the  $x$  axis indicates the area of the magphonic crystal; the acoustic wave is excited at point S; patterned areas are damping edges.

Without damping, the acoustic wave is completely transformed into spin wave at the distance  $3.4 \mu\text{m}$ , which is almost the same as predicted by CMT calculations. The energy is transferred back to the spin wave after the distance  $2L_{\text{tr}}$ . It is worth noting that while the wavelength of acoustic wave is about  $50 \text{ nm}$ , the wavelength of the spin wave is half that, about  $23 \text{ nm}$ .

The spin-wave loss length is about  $1 \mu\text{m}$  in permalloy ( $\alpha = 0.01$ ) and  $2 \mu\text{m}$  in CoFeB ( $\alpha = 0.004$ ) for the bulk wave at  $60 \text{ GHz}$ . Black dashed lines in Fig. 7(b) are the absolute amplitudes of acoustic wave and spin wave with the effect of damping. From this it is visible that the acoustic wave still excites the spin wave in the Py1/CoFeB structure and the maximum amplitude of the spin wave is twice smaller than without damping. Then, from the distance of  $3 \mu\text{m}$ , the amplitude of the SW decreases but it seems that it is not transferred back into acoustic wave.

The results of the time-domain simulations are compared with the CMT calculations, where the damping effect was taken into account by introducing complex spin wave number  $k = k_r + ik_i$ . The value of  $k_i$  is introduced to the calculations to be  $k_i = 1/\hat{L}_{\text{loss}} = 0.8 \mu\text{m}^{-1}$ , where  $\hat{L}_{\text{loss}}$  is the averaged loss length of the Py1/CoFeB structure. Figure 7 shows that the evolution of the acoustic mode and spin mode amplitudes obtained by CMT are in full agreement with that of FEM simulations.

The effect of damping onto the wave space distribution is shown again in Fig. 8 by comparing its amplitudes with that without damping. In case of codirectional coupling [Fig. 8(a)] it is seen that the excited spin-wave amplitude is decreased and it reaches its maximum value in a smaller distance, i.e.,  $x \approx 2 \mu\text{m}$ . However, the value of  $L_{\text{tr}}$  has actually increased since  $U(x)$  reaches zero at  $x \approx 10 \mu\text{m}$ . Further it grows again and reaches maximum for  $x \approx 12.5 \mu\text{m}$ , while  $M(x)$  reaches

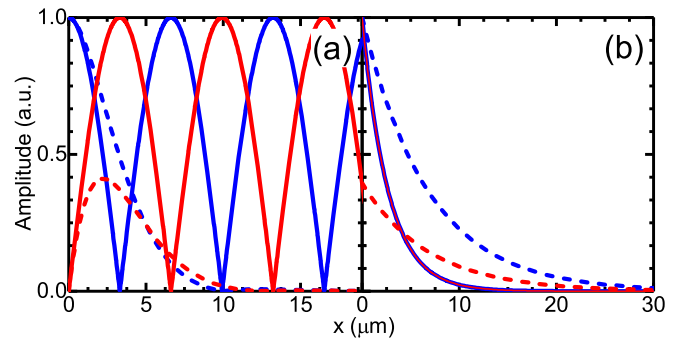


FIG. 8. Amplitudes  $U(x)$  (blue line) and  $M(x)$  (red line) in the Py1/CoFeB system without damping (solid lines) and with damping (dashed lines) in (a) codirectional coupling and (b) contra-directional C2 crossing.

minimum. However, the amplitudes of both modes become negligible above  $x \approx 10 \mu\text{m}$ .

While for a lossless system  $D$ ,  $\kappa$ ,  $\Delta\beta$ , and  $\bar{\beta}$  are either real or imaginary, they become complex if the complex value of  $k$  is introduced. Then, neither  $U(x)$  nor  $M(x)$  may be considered as a functions described by purely trigonometric or purely hyperbolic functions, as in the case of the codirectional and contradirectional couplings described in Secs. II A and II B. They are complex superposition of trigonometric functions describing mode energy transfer and exponential decay due to a damping. Therefore, the maximum value of  $M(x)$  is shifted to a smaller distance because of the exponential damping of the wave, despite the higher value of the transfer length. It is worth noting that while in the case of the asynchronous state the  $L_{\text{tr}}$  becomes smaller but the energy exchange is only partial, damping causes the increase of  $L_{\text{tr}}$  but modes exchange all of the energy which is not yet lost.

For completeness, in Fig. 8(b) we present  $M(x)$  and  $U(x)$  in the lossless and damped Py1/CoFeB system for the contradirectional crossing C2 [Fig. 7(a)]. It is seen that the distance required for almost full power exchange between modes is larger for the damped system and the outgoing spin wave has an amplitude that has been reduced by more than half.

#### IV. SUMMARY

The codirectional and contradirectional couplings between spin waves and acoustic waves in the magphonic crystal have been described. It is an active in-space mechanism which transfers energy between magnetic and mechanic degrees of freedom. Coupled mode theory formalism allows for quantitative description of the MEC strength. The structure has been optimized for an efficient and broadband codirectional coupling. In this case, magnetoelastic wave propagates through the magphonic crystal. The phenomenon may be utilized for a conversion of an acoustic wave to a spin wave or vice versa. For example, the Py1/CoFeB multilayer considered above should be of about  $2 \mu\text{m}$  thick to obtain maximum forward energy transfer to the spin wave at the output [Fig. 8(a)]. On the other hand, in contradirectional coupling the magphonic crystal thickness should be as thick as possible to obtain a



backward spin wave at the output (in case of acoustic wave at the input).

We have shown that it is possible to resonantly excite a spin wave by an acoustic wave in the case of bulk waves, where the damping is very strong. From Table I it is evident that YIG is the most promising candidate in the context of magnetoelastic coupling. The value of the transfer length is much less than the loss length. Furthermore, it should be possible to achieve this effect in thin films, since the loss lengths are much larger for magnetostatic surface and volume spin waves than for bulk exchange waves. Further engineering of the band structures in magphonic crystals together with the development of CMT

analysis for surface waves are required to optimize this effect.

#### ACKNOWLEDGMENTS

We thank Jarosław Kłos for valuable remarks during the preparation of the manuscript. The study has received financial support from the National Science Centre of Poland under Grants No. UMO-2012/07/E/ST3/00538 and No. UMO-2016/21/B/ST3/00452 and the EU's Horizon 2020 research and innovation programme under Marie Skłodowska-Curie GA No. 644348 (MagIC).

- 
- [1] A. Yariv and P. Yeh, *Optical Waves in Crystals* (John Wiley & Sons, New York, 2003).
- [2] A. Yariv, Coupled-Mode theory for guided-wave optics, *IEEE J. Quantum Electron.* **9**, 919 (1973).
- [3] K. Zhang and D. Li, *Electromagnetic Theory for Microwaves and Optoelectronics* (Springer-Verlag, Berlin, 2008).
- [4] Y. Sivan, S. Rozenberg, and A. Halstuch, Coupled-mode theory for electromagnetic pulse propagation in dispersive media undergoing a spatiotemporal perturbation: Exact derivation, numerical validation, and peculiar wave mixing, *Phys. Rev. B* **93**, 144303 (2016).
- [5] S. Khorasani and B. Rashidian, Coupled mode theory of waveguides with conducting interfaces, *Scientia Iranica* **10**, 426 (2003).
- [6] W.-P. Huang, Coupled-mode theory for optical waveguides: An overview, *J. Opt. Soc. Am.* **11**, 963 (1994).
- [7] H. Kogelnik and C. V. Shank, Coupled-wave theory of distributed feedback lasers, *J. Appl. Phys.* **43**, 2327 (1972).
- [8] V. L. Zhang, F. S. Ma, H. H. Pan, C. S. Lin, H. S. Lim, S. C. Ng, M. H. Kuok, S. Jain, and A. O. Adeyeye, Observation of dual magnonic and phononic bandgaps in bi-component nanostructured crystals, *Appl. Phys. Lett.* **100**, 163118 (2012).
- [9] H. Pan, V. L. Zhang, K. Di, M. H. Kuok, H. S. Lim, S. C. Ng, N. Singh, and A. O. Adeyeye, Phononic and magnonic dispersions of surface waves on a permalloy/BARC nanostructured array, *Nanoscale Res. Lett.* **8**, 115 (2013).
- [10] C. Kittel, Physical theory of ferromagnetic domains, *Rev. Mod. Phys.* **21**, 541 (1949).
- [11] R. L. Comstock and B. A. Auld, Parametric coupling of the magnetization and strain in a ferrimagnet. I. Parametric excitation of magnetostatic and elastic modes, *J. Appl. Phys.* **34**, 1461 (1963).
- [12] C. Kittel, Interaction of spin waves and ultrasonic waves in ferromagnetic crystals, *Phys. Rev.* **110**, 836 (1958).
- [13] L. Dreher, M. Weiler, M. Pernpeintner, H. Huebl, R. Gross, M. S. Brandt, and S. T. B. Goennenwein, Surface acoustic wave driven ferromagnetic resonance in nickel thin films: Theory and experiment, *Phys. Rev. B* **86**, 134415 (2012).
- [14] L. Thevenard, I. S. Camara, S. Majrab, M. Bernard, P. Rovillain, A. Lemaître, C. Gourdon, and J.-Y. Duquesne, Precessional magnetization switching by a surface acoustic wave, *Phys. Rev. B* **93**, 134430 (2016).
- [15] P. G. Gowtham, T. Moriyama, D. C. Ralph, and R. A. Buhrman, Traveling surface spin-wave resonance spectroscopy using surface acoustic waves, *J. Appl. Phys.* **118**, 233910 (2015).
- [16] P. G. Gowtham, D. Labanowski, and S. Salahuddin, The mechanical back-action of a spin-wave resonance in a magnetoelastic thin film on a surface acoustic wave, *Phys. Rev. B* **94**, 014436 (2016).
- [17] R. Sasaki, Y. Nii, Y. Iguchi, and Y. Onose, Nonreciprocal propagation of surface acoustic wave in Ni/LiNbO<sub>3</sub>, *Phys. Rev. B* **95**, 020407(R) (2017).
- [18] T. Kikkawa, K. Shen, B. Flebus, R. A. Duine, K.-I. Uchida, Z. Qiu, G. E. W. Bauer, and E. Saitoh, Magnon Polarons in the Spin Seebeck Effect, *Phys. Rev. Lett.* **117**, 207203 (2016).
- [19] C. Chen, A. Barra, A. Mal, G. Carman, and A. Sepulveda, Voltage induced mechanical/spin wave propagation over long distances, *Appl. Phys. Lett.* **110**, 072401 (2017).
- [20] J. Janušonis, T. Jansma, C. L. Chang, Q. Liu, A. Gatilova, and A. M. Lomonosov, Transient grating spectroscopy in magnetic thin films: Simultaneous detection of elastic and magnetic dynamics, *Sci. Rep.* **6**, 29143 (2016).
- [21] M. Fähnle, T. Tsatsoulis, C. Illg, M. Haag, B. Y. Müller, and L. Zhang, Ultrafast demagnetization after femtosecond laser pulses: Transfer of angular momentum from the electronic system to magnetoelastic spin-phonon modes, *J. Supercond. Novel Magn.* **30**, 1381 (2017).
- [22] J.-W. Kim and J.-Y. Bigot, Magnetization precession induced by picosecond acoustic pulses in a freestanding film acting as an acoustic cavity, *Phys. Rev. B* **95**, 144422 (2017).
- [23] J. V. Jager, A. V. Scherbakov, B. A. Glavin, A. S. Salasyuk, R. P. Champion, A. W. Rushforth, D. R. Yakovlev, A. V. Akimov, and M. Bayer, Resonant driving of magnetization precession in a ferromagnetic layer by coherent monochromatic phonons, *Phys. Rev. B* **92**, 020404(R) (2015).
- [24] M. Bombeck, J. V. Jäger, A. V. Scherbakov, T. Linnik, D. R. Yakovlev, X. Liu, J. K. Furdyna, A. V. Akimov, and M. Bayer, Magnetization precession induced by quasitransverse picosecond strain pulses in (311) ferromagnetic (Ga, Mn)As, *Phys. Rev. B* **87**, 060302(R) (2013).
- [25] M. Bombeck, A. S. Salasyuk, B. A. Glavin, A. V. Scherbakov, C. Brüggemann, D. R. Yakovlev, V. F. Sapega, X. Liu, J. K. Furdyna, A. V. Akimov, and M. Bayer, Excitation of spin waves in ferromagnetic (Ga, Mn)As layers by picosecond strain pulses, *Phys. Rev. B* **85**, 195324 (2012).
- [26] A. Kamra, H. Keshtgar, P. Yan, and G. E. W. Bauer, Coherent elastic excitation of spin waves, *Phys. Rev. B* **91**, 104409 (2015).
- [27] P. Graczyk, J. Kłos, and M. Krawczyk, Broadband magnetoelastic coupling in magnonic-phononic crystals for high-frequency

- nanoscale spin-wave generation, *Phys. Rev. B* **95**, 104425 (2017).
- [28] D. Stancil and A. Prabhakar, *Spin Waves* (Springer, Berlin, 2009).
- [29] A. Conca, J. Greser, T. Sebastian, S. Klingler, B. Obry, B. Leven, and B. Hillebrands, Low spin-wave damping in amorphous  $\text{Co}_{40}\text{Fe}_{40}\text{B}_{20}$  thin films, *J. Appl. Phys.* **113**, 213909 (2013).
- [30] M. Barthelmess, C. Pels, A. Thieme, and G. Meier, Stray fields of domains in permalloy microstructures—Measurements and simulations, *J. Appl. Phys.* **95**, 5641 (2004).
- [31] H. Alberts and L. Alberts, On the magnetization and magnetostriction of polycrystalline cobalt, *Physica* **31**, 1063 (1965).
- [32] C. Eyrych, W. Huttema, M. Arora, E. Montoya, F. Rashidi, C. Burrowes, B. Kardasz, E. Girt, B. Heinrich, O. N. Mryasov, M. From, and O. Karis, Exchange stiffness in thin film Co alloys, *J. Appl. Phys.* **111**, 07C919 (2012).
- [33] P. Hansen, Magnetostriction of ruthenium-substituted yttrium iron garnet, *Phys. Rev. B* **8**, 246 (1973).
- [34] D. Wang, C. Nordman, Z. Qian, J. M. Daughton, and J. Myers, Magnetostriction effect of amorphous CoFeB thin films and application in spin-dependent tunnel junctions, *J. Appl. Phys.* **97**, 10C906 (2005).
- [35] E. Klokholm and J. A. Aboaf, The saturation magnetostriction of permalloy films, *J. Appl. Phys.* **52**, 2474 (1981).
- [36] P. Pirro, T. Brächer, A. V. Chumak, B. Lägele, C. Dubs, O. Surzhenko, P. Gönert, B. Leven, and B. Hillebrands, Spin-wave excitation and propagation in microstructured waveguides of yttrium iron garnet/Pt bilayers, *Appl. Phys. Lett.* **104**, 012402 (2014).
- [37] J. Rychlý, J. W. Klos, and M. Krawczyk, Spin wave damping in periodic and quasiperiodic magnonic structures, *J. Phys. D: Appl. Phys.* **49**, 175001 (2016).
- [38] W. P. Mason, Phonon viscosity and its effect on acoustic wave attenuation and dislocation motion, *J. Acoust. Soc. Am.* **32**, 458 (1960).
- [39] R. Lifshitz and M. L. Roukes, Thermoelastic damping in micro- and nano-mechanical systems, *Phys. Rev. B* **61**, 5600 (2000).